Scaling Characteristics of the XeF ($C \rightarrow A$) Excimer Laser

C. BRENT DANE, GRAEME J. HIRST, SHIGERU YAMAGUCHI, THOMAS HOFMANN, WILLIAM L. WILSON, JR., SENIOR MEMBER, IEEE, ROLAND SAUERBREY, MEMBER, IEEE, FRANK K. TITTEL, FELLOW, IEEE, WILLIAM L. NIGHAN, SENIOR MEMBER, IEEE, AND MICHAEL C. FOWLER

(Invited Paper)

Abstract—**The scaling characteristics and medium properties of an injection controlled XeF($C \rightarrow A$) laser pumped by a 10 ns high current density electron beam have been investigated. A five-component laser gas mixture consisting of F_2, NF_3, Xe, Kr, and Ar was optimized for the scaled laser conditions resulting in 0.8 J output pulses at 486.8 nm, corresponding to an energy density of 1.7 J/L and an intrinsic efficiency of 1.3%. Detailed small-signal-gain measurements combined with kinetic modeling permitted the characterization of the dependence of net gain on the electron beam energy deposition and gas mixture composition, resulting in an improved understanding of XeF($C \rightarrow A$) laser operation.**

I. Introduction

THERE is increasing interest in the XeF($C \rightarrow A$) excimer laser as an efficient, tunable source of radiation in the blue-green region of the spectrum. Using an electron beam as an excitation source and a *kinetically tailored* five-component gas mixture [1], efficient operation of this laser system has been demonstrated for short pulse 10 ns, ~ 10 MW/cm^3 [2], intermediate pulse 250 ns, ~ 1 MW/cm^3 [3], and long pulse 700 ns, ~ 250 kW/cm^3 [4] electron beam pumping durations. When the short pulse, high current density electron beam excitation technique is employed, peak values of small-signal gain exceed 3%/cm permitting efficient injection-controlled operation using a low-power injection beam. This results in narrow-band high beam quality operation and provides a very effective method for wavelength tuning. Continuous tuning between 450 and 530 nm has been demonstrated, and an output energy density of >1 J/L has been achieved for wavelengths between 470 and 510 nm [5].

With its gaseous active medium, the XeF($C \rightarrow A$) excimer laser is readily scalable to the high energy and power required for applications in remote sensing, materials processing, optical communications, and the amplification of ultrashort laser pulses. Experiments are described here that characterize the successful scaling of a high current density electron beam pumped XeF($C \rightarrow A$) laser from an active volume of ~ 0.02[6] to one of ~ 0.5 L. The effect of the scaled volume on the optimum laser gas mixture composition is considered in detail. Through a careful mapping of the spatial distribution of electron beam energy deposition, the relationship between kinetic processes, small-signal gain, and laser performance has been determined in order to identify optimum pumping conditions.

Manuscript received December 1, 1989; revised March 19, 1990. This work was supported by the Office of Naval Research, the Robert Welch Foundation, and the National Science Foundation.

C. B. Dane, G. J. Hirst, S. Yamaguchi, T. Hofmann, W. L. Wilson, R. Sauerbrey, and F. K. Tittel are with the Department of Electrical and Computer Engineering, Rice University, Houston, TX 77251.

W. L. Nighan and M. C. Fowler are with the United Technologies Research Center, East Hartford, CT 06108.

IEEE Log Number 9037368.

II. Experimental Apparatus

A. Electron Beam Pumping

The XeF($C \rightarrow A$) excimer laser was transversely pumped by a pulsed (10 ns FWHM), high current density electron beam customized for this application [7]. Electrons were emitted from a 50 cm · 2 cm carbon felt cathode through a 25 μm titanium foil window into the laser gas mixture as illustrated in Fig. 1. Typical diode peak voltage and current were 650 kV and 80 kA, respectively. Using a Faraday probe, a peak current density of ~ 150 A/cm^2 was measured on the optical axis when the laser cell was filled with 6.5 bar of Ar (Fig. 2). The electron beam system is capable of repetitive operation at up to 1 Hz.

The spatial distribution of the electron beam energy deposition in the gas was measured using chlorostyrene film [8]. For a typical laser gas mixture, an average of 150 J/L was deposited on the optical axis of the laser cell with $\pm 15\%$ variations from this average along the 50 cm pumped length (Fig. 3). The slight roll-off in energy deposition away from the center of the cell was due in part to a $\sim 1°$ rotation of the electron beam caused by a 0.2 T magnetic field used to guide the electron beam. The use of this guide field resulted in a threefold increase in the electron current delivered at the optical axis.

As expected, the energy deposition varied significantly in the direction of the electron beam propagation due to

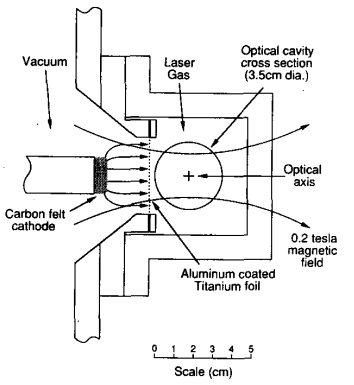

Fig. 1. Cross-sectional view of the electron beam pumped laser cell. Electrons are emitted from the 2 cm wide × 50 cm long carbon felt cathode across the 2.2 cm anode-cathode gap. The hibachi support ribs and the back of the titanium foil serve as the anode. For these experiments, the optical resonator diameters were 3.5 cm resulting in an active laser volume of 0.48 L.

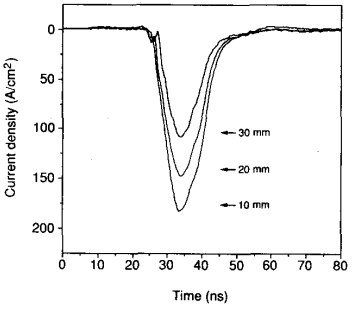

Fig. 2. Temporal current density profiles measured inside the laser cell using a Faraday probe with a diameter of 3.8 mm. The probe was positioned 10, 20, and 30 mm from the foil. Attenuation was the result of scattering and energy deposition in the 6.5 bar gas mixture. Peak values of ~150 A/cm² were observed on the optical axis (20 mm) with a FWHM of 10 ns.

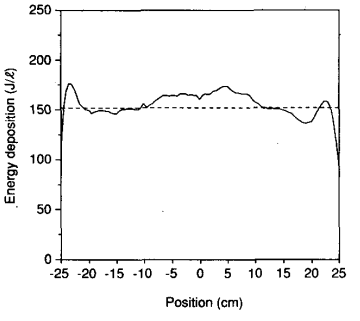

Fig. 3. Energy deposition profile along the optical axis (20 mm from the titanium foil) as measured by chlorostyrene film. Typically, ±15% variations were observed from an average value (denoted by a dashed line) of ~150 J/L. The slight roll off in energy deposition from the center of the laser cell was due in part to a ~1° rotation of the electron beam by the 0.2 T magnetic guide field.

electron energy loss and scattering in the 6.5 bar laser gas mixture. The deposition ranged from over 200 J/L near the foil to less than 100 J/L at the back wall of the laser cell. A contour plot of the measured energy deposition through a cross section near the center of the cell, as experimentally measured with chlorostyrene film, is shown in Fig. 4. For an active laser volume 3.5 cm in diameter and 50 cm long (0.48 L), the electron beam energy deposition was typically ~125 ± 10 J/L, averaged over this volume. A pressure transducer installed in the laser cell was used to measure the transient pressure rise following an electron beam pumping pulse, resulting in energy depositions consistent (±10%) with the integrated chlorostyrene film measurements [9].

B. Laser Cell and Resonator

The laser cell and gas handling system were constructed entirely of stainless steel using Viton and Teflon vacuum seals. The surface of the titanium foil in contact with the laser gas was coated with a 5 μm thick layer of aluminum using ion vapor deposition. This coating prevented interaction between the titanium and the fluorine and was found to significantly increase the lifetime of the gas mixtures. The laser gas mixture components were introduced into the cell sequentially, and then mixed by circulating them through an external loop at 1 L/min using a small high-pressure bellows pump. The cell, electron beam foil, and gas handling systems were initially passivated by filling the system with 3 bar of a 10% F_2 in Ar gas mixture for a period of 24 h.

The optical cavity configuration used in these experiments was a positive branch confocal unstable resonator. The back reflector was a plano-concave lens with the concave surface (radius of curvature = R_1) coated to achieve maximum reflectivity from 465 to 505 nm. This coating was also designed to allow greater than 80% transmission near the ~350 nm wavelength of the competing XeF($B \rightarrow X$) transition. A 1.5 mm injection aperture, centered on the back reflector, was formed either by drilling a hole through the optical substrate or by masking a 1.5 mm spot during the coating process. The latter method was found to provide the most well defined aperture and became the preferred technique. The output coupler was a double meniscus lens (radii of curvature = R_2, $-R_2$) with a round maximum reflectivity spot centered on the convex surface. For each cavity magnification (R_1/R_2), the size of this spot was chosen such that the outer diameter of the laser beam, given by the product of the spot diameter and the magnification, was ~35 mm. The distance between the mirrors was adjusted to the confocal spacing of $(R_1 - R_2)/2$.

Two resonator configurations were used in these experiments. In the first, the cavity mirrors were located inside the laser cell in contact with the gas mixture on externally adjustable mounts. The optical coatings were protected from the corrosive laser gases by an aluminum oxide overcoating. In the second configuration, the mirrors were located *outside* the laser cell, which was sealed with antireflection-coated fused silica windows tilted by 3°. The internal resonator had a magnification of 1.7 (R_1 = 2.73 m, R_2 = 1.61 m), an output coupler spot diameter of 21 mm, and a mirror spacing of 56 cm. This magnification

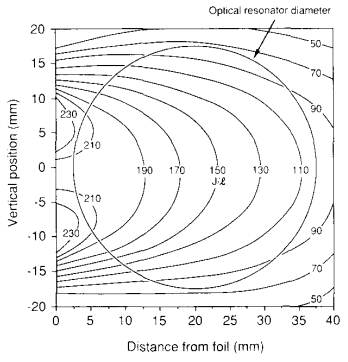

Fig. 4. Constant energy deposition contours through a cross section near the center of the laser cell measured using chlorostyrene film. An average deposition of 142 J/L was measured for this cross section of the optical resonator corresponding to an average of ~125 J/L for the entire 0.48 L resonator volume. This resulted in a total deposited energy of ~60 J in the active laser medium.

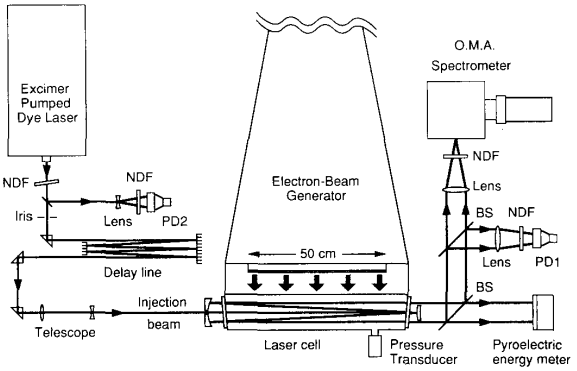

Fig. 5. A schematic of the experimental layout showing energy, temporal, and spectral diagnostics. The laser cell in this case is shown with *external* resonator optics. OMA: optical multichannel analyzer. PD: vacuum photodiode. NDF: neutral density filter. BS: uncoated fused silica beamsplitter.

was chosen to optimize the peak power and near-field output energy of the scaled XeF($C \rightarrow A$) laser [10]. Gas mixture optimization experiments were performed using a 75 cm long *external* resonator with a magnification of 2.0 ($R_1 = 3.00$ m, $R_2 = 1.50$ m) and an output coupler spot diameter of 17.5 mm.

C. Injection Source

A dye laser pumped by a 60 ns FWHM XeCl excimer laser provided a 45 ns FWHM injection pulse with a linewidth of ~0.005 nm as measured using a monitor etalon with a finesse of 30 and a free spectral range of 30 GHz [5]. The relatively long pulsewidth allowed the unstable resonator to be completely filled with injected photons before the onset of gain resulting in quasi-CW injection. The beam diameter was adjusted with a telescope so that the 1.5 mm injection hole was uniformly illuminated, transmitting approximately 60% of the injection pulse into the optical cavity. The injection intensity was varied using neutral density filters at the dye laser output. With no attenuation, it was possible to deliver ~2 mJ through the unstable resonator injection hole corresponding to a peak intensity of ~3 MW/cm^2, a value close to the ~5-6 MW/cm^2 saturation intensity of the XeF($C \rightarrow A$) transition.

For a well-aligned system, a portion of the injection beam was backreflected through the injection aperture along the same path as the incoming beam. The amplification of this backreflected pulse in the dye laser gain cell resulted in the truncation of the outgoing injection pulse as well as damage to optical components of the dye laser. To avoid this difficulty, an optical delay line was used to increase the round-trip transit time between the injection source and the electron beam pumped amplifier to 40 ns.

D. System Diagnostics

The diagnostics system was designed to extensively characterize the operation of both the XeF($C \rightarrow A$) laser and the electron beam generator on each laser shot. As depicted in Fig. 5, the laser output temporal profile was measured by a vacuum biplanar photodiode, the spectral profile by an optical multichannel analyzer (OMA) spectrometer, and the energy by a pyroelectric energy meter. A second photodiode was used to monitor the dye laser injection control pulse. Electron beam diagnostics consisted of voltage and current monitors in the diode and a Marx bank charging voltage monitor. The shot-to-shot energy deposition in the laser gas was monitored using the signal from the pressure transducer which was calibrated against the chlorostyrene film measurements. The signal from the photodiode monitoring the XeF($C \rightarrow A$) output was recorded using a 500 MHz scan-converting transient digitizer and the remaining temporal signals were collected using a four-channel 400 Msample/s and a two-channel 10 Msample/s digital oscilloscope. A single computer system configurated the instruments and collected each of the diagnostic signals for each laser shot.

III. Gas Mixture Optimization

The first experiments with the scaled injection controlled XeF($C \rightarrow A$) laser system were performed using a five-component gas mixture which had been previously optimized for a small-scale laser having a similar electron beam pumping rate but with a 10 cm active length and a volume of only 0.02 L [6]. That gas mixture was comprised of 8 torr NF_3, 1 torr F_2, 8 torr Xe, 300 torr Kr, and Ar, with a total pressure of 6.5 bar. In our prior work, the dual halogen donor, dual rare gas buffer composition was found to result in a significant reduction in transient blue-green absorption and the suppression of the competing XeF($B \rightarrow X$) transition [1]. Detailed kinetic modeling successfully described this performance enhancement and accurately predicted small-signal-gain profiles for a variety of laser gas mixtures and electron beam pumping conditions [11]. However, the scaling of the active medium length from 10 m to 50 cm introduced an additional factor affecting the optimum XeF($C \rightarrow A$) laser gas mixture.

A. KrF($B \rightarrow X$) Competition

The presence of Kr as a buffer in the laser gas results in the formation of the KrF excimer. Indeed, modeling indicates a KrF($B \rightarrow X$) gain on the order of 10%/cm for mixture conditions otherwise optimum for XeF($C \rightarrow A$) laser operation. Nonetheless, for the short 10 cm single-pass gain length and resonator optics having low reflectivities at 248 nm, no KrF lasing was observed for conditions typical of the earlier small-scale experiments [6]. However, when the gain length was scaled by a factor of five to 50 cm, oscillation on the KrF($B \rightarrow X$) laser transition occurred, using the mixture optimized for the small-scale experiment. This resulted in significant laser output at 248 nm and a reduction in the XeF($C \rightarrow A$) gain. The primary adverse effect of KrF oscillation on XeF($C \rightarrow A$) laser output is the reduction in the population of Kr_2F, a major XeF(C) precursor [1], [11]. Since KrF is the precursor of Kr_2F, strong stimulated emission on the KrF($B \rightarrow X$) transition results in lower KrF, Kr_2F, and XeF(C) populations.

Using the gas mixture optimized for the small-scale experiments, along with the internally-mounted $M = 1.7$ resonator and an injection intensity of ~ 2 MW/cm^2 at 486.8 nm, 0.6 J laser output pulses were measured in the first tests of the scaled laser system. Spectral analysis revealed that the laser output consisted of output at the amplified injection wavelength as well as at the 248 nm wavelength of the KrF transition. Using a Corning 3-74 filter to block the UV portion of the output (cutoff at $\sim$420 nm), it was determined that $\sim$0.45 J was emitted at 486.8 nm and $\sim$0.15 J at 248 nm. An examination of the temporal profiles depicted in Fig. 6 shows that the KrF gain and laser output occurs much earlier than those of the XeF($C \rightarrow A$) transition. As might be expected from this fact, the energy of the UV pulse was independent of the performance of the XeF($C \rightarrow A$) laser. If the visible injection was omitted, the XeF($C \rightarrow A$) laser produced only $\sim$0.03 J free-running output but the UV output was unaffected. For the conditions of Fig. 6, the 248 nm pulse and the free-running blue–green pulse were collected during the same shot and the injection controlled pulse was recorded on a subsequent laser shot.

Fig. 7 shows the measured Kr pressure dependence of the output of the injection controlled XeF($C \rightarrow A$) amplifier at 486.8 nm, along with the XeF($B \rightarrow X$) and KrF($B \rightarrow X$) lasers at 351 and 248 nm, respectively. At the 300 torr Kr pressure found to be optimum for XeF($C \rightarrow A$) laser operation in our earlier small scale experiments, the KrF laser output reaches its maximum value and the scaled XeF($C \rightarrow A$) output exhibits a pronounced dip. However, the data of Fig. 7 show that the laser output from the KrF transition is easily suppressed by increasing the partial pressure of Kr in the gas mixture above 300 torr, with a maximum in XeF($C \rightarrow A$) output occurring at a Kr pressure of 1200 torr. For Kr pressures greater than 1000 torr, the UV output is almost completely suppressed. Using a gas mixture comprised of 8 torr NF_3, 1 torr F_2, 8 torr Xe, and 1200 torr Kr, completed to 6.5 bar with Ar, injection

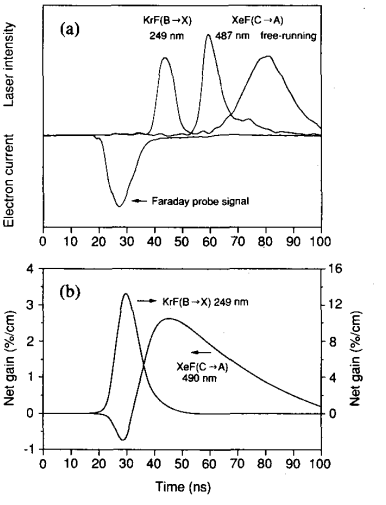

Fig. 6. (a) Output pulses observed from the XeF($C \rightarrow A$) laser using an $M = 1.7$ internal resonator and the gas mixture previously optimized for the small-scale laser [6]. The mixture was comprised of 8 torr NF_3, 1 torr F_2, 8 torr Xe, 300 torr Kr, and completed to 6.5 bar using an Ar buffer. The pulses are displayed on an arbitrary vertical scale; their relative sizes do not reflect actual relative intensities. An energy of $\sim$0.15 J was measured for the KrF($B \rightarrow X$) pulse and $\sim$0.45 J for the injection controlled XeF($C \rightarrow A$) pulse. For the purpose of comparison, the temporal evolution of the $\sim$0.03 J broad-band free-running XeF($C \rightarrow A$) laser is also shown. The KrF($B \rightarrow X$) and XeF($C \rightarrow A$) free-running laser temporal profiles were measured for the same electron beam shot. The injection-controlled output and the Faraday probe signal were measured on separate shots. Temporal synchronization was ensured by triggering the transient digitizer with the signal from the diode voltage monitor of the electron beam generator. (b) Computed temporal evolution of the KrF($B \rightarrow X$) and XeF($C \rightarrow A$) small-signal-gain profiles for typical experimental conditions.

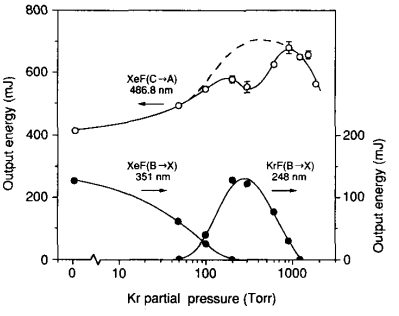

Fig. 7. Laser output energies at the XeF($C \rightarrow A$), XeF($B \rightarrow X$), and KrF($B \rightarrow X$) wavelengths for the injection controlled laser using an internal $M = 1.7$ resonator. The gas mixture, optimized for the small-scale experiments, consisted of 8 torr NF_3, 1 torr F_2, 8 torr Xe, and was completed to 6.5 bar using an Ar buffer. An obviouis decrease occurs in the XeF($C \rightarrow A$) output at the Kr pressure for which peak in KrF($B \rightarrow X$) oscillation is observed. A Kr pressure of $\sim$300 torr was found to be optimum in the small-scale apparatus in which KrF($B \rightarrow X$) competition was not significant [6]. Modeling shows that for this mixture both the XeF($C \rightarrow A$) and KrF($B \rightarrow X$) gain reach their maximum value for this Kr pressure. The dashed line represents an estimated projection of XeF($C \rightarrow A$) laser performance in the *absence* of the KrF($B \rightarrow X$) laser competition.

controlled pulses were obtained with energies of 0.7 J [2]. The injection laser was tuned to 486.8 nm, a wavelength near the peak of the spectral gain profile. For the 0.48 L

active laser volume and a measured spatially-averaged energy deposition of 120 J/L, this corresponded to an energy density of 1.5 J/L and an intrinsic efficiency of 1.2%, respectively [2].

B. Scanning of Gas Mixture Components

Although the competing KrF laser oscillation was suppressed by increasing the Kr pressure to 1200 torr, the NF_3, F_2, and Xe partial pressures were not reoptimized. Thus a systematic optimization of the laser gas mixture was undertaken in order to maximize the XeF($C \rightarrow A$) laser extraction efficiency. A second requirement, of course, was the continued suppression of the KrF($B \rightarrow X$) laser. Pyroelectric energy meters were chosen to monitor the laser output at the injected and UV wavelengths since quantitative measurements using the OMA spectrometer were complicated by the spectral response of the detector array and by differences in beam size and collimation between the blue-green and UV laser output. A schematic of the measurement system using two pyroelectric energy meters, one of which was equipped with a filter to block 248 nm is shown in Fig. 8. The signal from detector *A* was corrected for losses from the uncoated fused silica beamsplitter and the UV filter. By removing the UV filter the signal from detector *B* was then calibrated against that from *A*. In this manner, the visible (*A*) and UV (*B*–*A*) were measured for each laser shot. Since the UV measurement was the difference of two larger measurements, small negative values sometimes resulted for UV output energies near zero.

For the purpose of these measurements, the *external* unstable cavity was used in order to ensure long term stability of the resonator coatings. However, the intracavity losses introduced by the laser cell windows and increased unpumped cavity length resulted in XeF($C \rightarrow A$) laser energies somewhat smaller than those observed with the internal resonator, as predicted [10]. An injection pulse at 486.8 nm with a peak intensity of ~ 2 MW/cm^2 was used in all cases. Although the laser output was much more sensitive to small changes in the net gain for the linear, unsaturated amplification regime resulting from smaller injection intensities, this intensity was chosen for these experiments to ensure that the laser system was optimized under the conditions for which saturation of both gain and absorber species occurred. The partial pressure of each gas component was scanned, leaving the other component pressures fixed, to determine the value for which the XeF($C \rightarrow A$) laser energy was optimized. The concentration of that constituent was then fixed at a value near the measured optimum before the next gas component was scanned. In this manner, two iterations were made through the NF_3, F_2, Xe, and Kr mixture components, always maintaining a total laser gas pressure of 6.5 bar with the Ar buffer. Small variations were then made from the final gas mixture by simultaneously changing the concentration of two or more components to verify that a performance peak had been achieved.

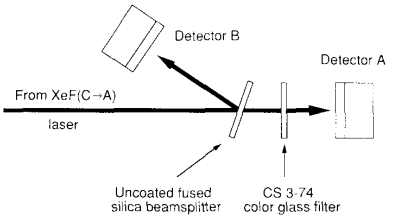

Fig. 8. Schematic of the two pyroelectric energy meter setup for measuring the blue-green and UV output of the laser system. A Corning CS 3-74 color glass filter with a cutoff at 420 nm and 88% transmission at 486.8 nm was used to filter out the UV from the light reaching detector *A*. The signal from *A* was corrected for losses from the beamsplitter and UV filter. The signal from *B* was then cross calibrated against that from *A* with the UV filter removed. The sensitivity of the energy meters at 248 nm differed by less than 10% from that in the blue-green.

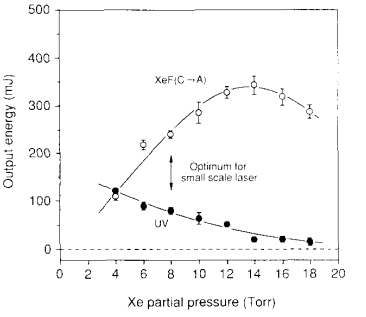

Fig. 9. Laser output energies at 486.8 nm (open circles) and in the UV (filled circles) as a function of Xe partial pressure measured as described in Fig. 8. The gas mixture consisted of 8 torr NF_3, 1 torr F_2, 300 torr Kr, and was completed to 6.5 bar using an Ar buffer. The *external* $M = 2$ resonator was used with a ~ 2 MW/cm^2 injection pulse at 486.8 nm. The error bars denote the standard deviation of the measured scatter for a given set of experimental conditions and do not include the $\pm 10\%$ absolute uncertainty in the calibration of the energy meters. The arrow indicates the optimum Xe pressure for the small-scale laser.

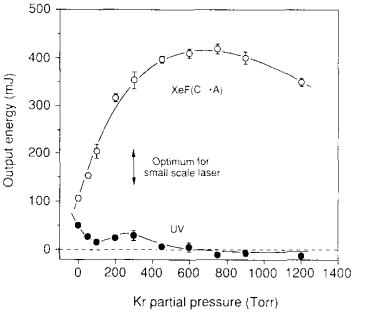

Fig. 10. Laser output energies at 486.8 nm (open circles) and in the UV (filled circles) as a function of Kr partial pressure. The Xe partial pressure was set at 14 torr, the observed maximum from Fig. 9. The remaining gas mixture consisted of 8 torr NF_3, 1 torr F_2, and was completed to 6.5 bar using an Ar buffer. The increase in Xe pressure from 8 to 14 torr reduced the Kr pressure required to completely suppress the KrF($B \rightarrow X$) output from 1200 torr [2] to ~ 500 torr. The arrow indicates the optimum Kr pressure for the small-scale laser.

Figs. 9–12 show the measured XeF($C \rightarrow A$) laser energy at 486.8 nm and the total UV laser energy for variations in Xe, Kr, NF_3, and F_2, respectively. Five to six

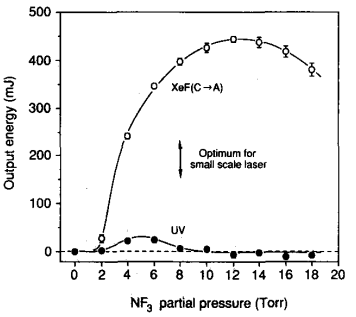

Fig. 11. Laser output energies at 486.8 nm (open circles) and in the UV (filled circles) as a function of NF_3 partial pressure. The gas mixture consisted of 1 torr F_2, 14 torr Xe, 450 torr Kr, and was completed to 6.5 bar using an Ar buffer. The arrow indicates the optimum NF_3 pressure for the small-scale laser.

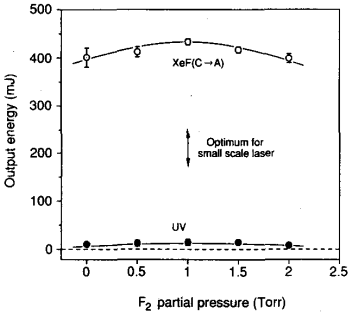

Fig. 12. Laser output energies at 486.8 nm (open circles) and in the UV (filled circles) as a function of F_2 partial pressure. The gas mixture consisted of 12 torr NF_3, 14 torr Xe, 450 torr Kr, and was completed to 6.5 bar using an Ar buffer. The increased optimum NF_3 pressure for the scaled XeF($C \rightarrow A$) laser system over that of R [6] reduced the sensitivity of laser performance to the F_2 partial pressure but a measurable improvement was still observed at ~ 1 torr. The arrow indicates the optimum F_2 pressure for the small-scale laser.

measurements using the same laser gas fill were averaged for each data point shown. The error bars represent the standard deviation of the scatter of the measured energies for a given set of conditions. This scatter was largely a result of small differences in injection laser synchronization, resonator alignment, and gas mixture lifetime. For this reason more representative values probably lie nearer the top of each bar than the center. The absolute accuracy of the measurements was limited in most cases by the pyroelectric energy meter calibration of $\pm 10\%$, an uncertainty not represented in the error bars.

The KrF($B \rightarrow X$) laser output was easily quenched by increasing the partial pressure of Xe in the gas mixture as shown in Fig. 9. However, an increase in the Xe concentration beyond a level at which the UV output is almost completely suppressed results in reduced blue–green output from the XeF($C \rightarrow A$) laser due to the increased quenching of XeF by Xe and broad-band absorption from the photoionization of Xe($5d$) and ($6p$) [1], [11]. When the Xe partial pressure was fixed at the observed performance maximum of 14 torr, the optimum Kr pressure

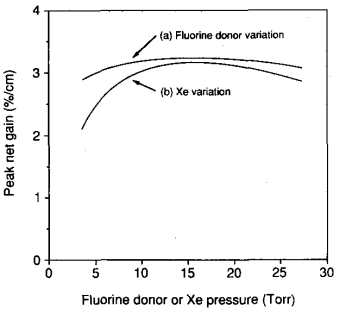

Fig. 13. Computed dependence of the peak XeF($C \rightarrow A$) gain at 490 nm with variation of either the fluorine donor or Xe partial pressure. The gas mixtures were comprised of (a) 12 torr Xe, 750 torr Kr, Ar to complete the mixture to a total pressure of 6.5 bar, with the total fluorine donor pressure varied while maintaining an 8 : 1 NF_3–F_2 ratio; and (b) 9 torr fluorine donor pressure with an 8 : 1 NF_3–F_2 ratio, 750 torr Kr, Ar to complete the mixture to 6.5 bar, with the Xe pressure varied. The electron beam pumping conditions were similar to those of Figs. 9–12.

(Fig. 10) decreased to ~ 750 torr from 1200 torr [2]. The optimum XeF($C \rightarrow A$) laser output was found at higher NF_3 pressures (Fig. 11) than used on the small scale system [6] resulting in less sensitivity to the F_2 concentration (Fig. 12). However, improved laser output continued to result from the addition of ~ 1 torr of F_2. The findings of the gas constituent scanning experiments are consistent with the small-signal gain computed using our XeF($C \rightarrow A$) laser kinetics model, described in detail elsewhere [11]. Fig. 13 shows the computed peak value of the XeF($C \rightarrow A$) net gain at 490 nm for variations in the Xe and fluorine donor partial pressures. Broad maxima in the computed gain are observed for Xe and fluorine donor pressures in the 10–20 torr range, a result consistent with the experimental data of Figs. 9, 11, and 12.

Fig. 14 shows the computed dependence of peak XeF($C \rightarrow A$) net gain on Kr partial pressure. In earlier work [1], analysis of the dependence of XeF($C \rightarrow A$) fluorescence decay and laser energy on Kr pressure resulted in an inferred rate coefficient of $\sim 1.0 \cdot 10^{-32}$ s^{-1} cm^6 for the three-body quenching reaction, XeF(C) + Kr + Ar $\rightarrow$ products. This rate coefficient is parameterized in the presentation of Fig. 14. Clearly, a rate coefficient very nearly equal to the $\sim 1.0 \cdot 10^{-32}$ s^{-1} cm^6 value inferred earlier is consistent with the experimental observation of a broad maximum in XeF($C \rightarrow A$) laser energy for Kr partial pressure in the 450–900 torr range (Fig. 10).

C. Results of Mixture Optimization

On the basis of the constituent scanning experiments, an optimized gas mixture consisting of 12 ± 2 torr NF_3, 1 ± 0.5 torr F_2, 12 ± 2 torr Xe, and 750 ± 150 torr Kr, completed with Ar to a total pressure of 6.5 bar, was determined for the scaled XeF($C \rightarrow A$) electron beam pumped laser system. Using this mixture, laser output energies in excess of 0.8 J at 486.8 nm were measured from the system with the *internal* resonator, corresponding to an intrinsic efficiency of 1.3% and an energy den-

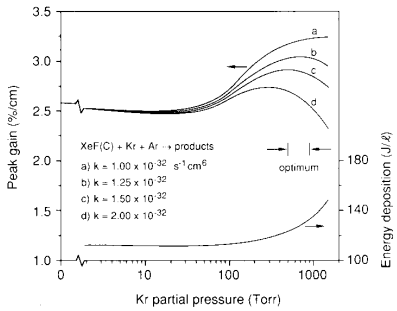

Fig. 14. Computed variation of the peak XeF($C \rightarrow A$) gain at 490 nm as a function of Kr pressure. The mixture was comprised of 12 torr Xe, 12 torr fluorine donor (8 : 1 NF_3–F_2 ratio), with Ar to complete the 6.5 bar mixture. The rate coefficient for Kr three-body quenching of XeF(C) is parameterized as described in the text. Also shown is the effect of Kr addition on the electron beam energy deposition (125 J/L at ~750 torr Kr).

sity of 1.7 J/L. The most significant aspect of the laser gas mixture modification performed upon scaling from a 0.02 to a 0.5 L active laser volume was the competition by the KrF($B \rightarrow X$) laser which was suppressed in a straightforward manner by the described mixture adjustments. The basic composition of the laser gas mixture remained very similar to those of previous laser experiments, and the behavior of the scaled system continued to be consistent with the current understanding of the kinetics of the XeF($C \rightarrow A$) multicomponent gas mixture [11].

IV. Gain Measurements

A. Gain Measurement Technique

The scaled electron beam pumped laser system with its uniformly excited 50 cm active length provided the opportunity for more accurate small-signal-gain measurements than were possible using the small-scale apparatus [6]. The interpretation of previous measurements was complicated by the small 10 cm pumped length over which the electron beam energy deposition varied by more than a factor of three from each end to the center. Aside from the need for detailed gain measurements for use as input data for analytical modeling of the injection control process [10], [12], a careful study of the dependence of gain on energy deposition into the laser gas mixture is required to investigate the optimum electron beam pumping intensity.

A flashlamp-pumped dye laser with a pulsewidth of ~200 ns was used as a gain probe in these experiments. The output was tuned to 486.8 nm and the peak intensity was attenuated to ~50 W/cm^2 using neutral density filters to avoid saturation effects in the gain medium. The diameter of the probe was adjusted to 2 mm and was aligned on the vertical center of the gain region, parallel to the titanium foil electron beam window. As described previously, an energy deposition gradient existed from the foil to the back of the laser cell due to the attenuation of the electron beam as it propagated through the high-pressure gas (Fig. 4). This was used to advantage since, by translating the probe beam along the direction of electron beam propagation, gain could be measured as a function of electron beam energy deposition. The gain signals were measured using a vacuum photodiode and consisted of the temporally-broad dye laser probe background onto which was superimposed the net gain profile. The largest source of uncertainty in the measurement of the peak net gain was in the estimation of the shape of the dye laser profile during the XeF($C \rightarrow A$) gain pulse.

B. Temporal Profiles

The measured net gain curves were found to be very similar to those obtained using the small previously reported 0.02 L device [6], exhibiting peak gains of ~3%/cm with a ~25 ns FWHM. Fig. 15 illustrates typical temporal profiles and the significant reduction of the transient absorption that occurs during the electron beam pumping pulse as Kr is added to the mixture. The XeF($C \rightarrow A$) peak gain was observed to be much less sensitive to the Kr partial pressure than the output energy of the injection controlled laser (Fig. 10). This, it is believed, can be attributed to two effects. First, although the dye laser injection pulse is much longer (~40 ns) than the gain pulse, when there is strong absorption during electron beam pumping (low Kr partial pressure), essentially all of the injected photons are removed from the cavity. Since the unstable resonator cannot be refilled with injection flux before the net gain reaches its peak, the extraction efficiency is reduced. Secondly, during the small-signal-gain measurements, the absence of a laser resonator resulted in reduced oscillation on the KrF($B \rightarrow X$) and XeF($B \rightarrow X$) transitions. As described in the previous section, these are in direct competition with the XeF($C \rightarrow A$) laser output (Fig. 7) and are effectively suppressed by the use of higher Kr partial pressures.

Fig. 16 shows computed temporal gain profiles for conditions similar to those of Fig. 15. Generally, the agreement between the measured and computed temporal profiles is very good. However, modeling indicates a larger reduction in the strong absorption during the electron beam beam pulse with increasing pressures of Kr. The absorption with no Kr in the mixture is believed to be due primarily to photodissociation of Ar_3^+ [1], [11]. The addition of Kr reduces the concentration of Ar_3^+ and its Ar_2^+ precursor by charge exchange. Since there is practically no rate coefficient data for Ar_3^+, known rate coefficients for Ar_2^+ were used in the modeling of Ar_3^+ [11], including the rate coefficient for Ar_3^+ – Kr charge exchange. This is one possibility for the discrepancy. Also, in the region of initial absorption, the computed net gain is the difference between two larger quantities, the XeF(C) contribution to gain and the absorption due to Ar_3^+ and other species. Thus, the computed net gain is subject to larger errors during the electron beam pumping than those typical in the afterglow region for which agreement between theory and experiment is very good.

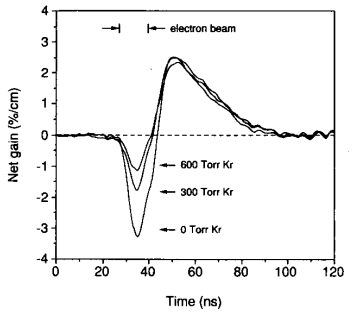

Fig. 15. Typical net gain temporal profiles measured using the 200 ns flashlamp-pumped dye laser probe tuned to 486.8 nm and directed along the optial axis of the laser cell. A strong absorption exists during the electron beam pumping pulse which is significantly reduced by the addition of Kr [1], [11]. For these measurements, the gas mixture consisted of 8 torr NF_3, 1 torr F_2, 8 torr Xe, and was completed to 6.5 bar using an Ar buffer.

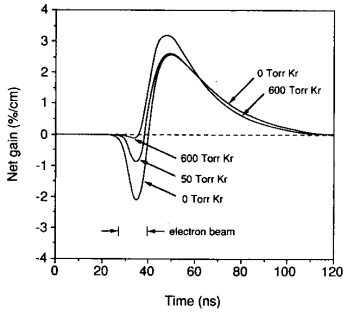

Fig. 16. Computed temporal variation of the net gain at 490 nm. The mixture was comprised of 12 torr fluorine donor (8:1 NF_3–F_2 ratio), Kr, and Ar for a total pressure of 6.5 bar. The electron beam pumping conditions were similar to those of Figs. 9–15.

C. Gain and Laser Energy Dependence on Pumping Intensity

Using the gas mixture optimized for the scaled XeF($C \rightarrow A$) amplifier as described in the previous section, gain measurements were made along the direction of the optical axis at distances between 2 and 40 mm from the foil electron beam window where each position corresponded to a different energy deposition level. With spatially resolved deposition measurements, such as those presented in Fig. 4, it was then possible to plot the peak net gain versus energy deposition. Fig. 17 shows measurements for two different laser gas mixtures. Also shown in the figure are calculated values of gain versus energy deposition. Clearly, the qualitative and quantitative agreement between theory and experiment is good, with the differences between the two within the uncertainty of each. Previous measurements on the small-scale electron beam device indicated the onset of gain saturation for a volume averaged deposition level of ~80 J/L with a peak in the intrinsic laser efficiency occurring at ~90 J/L [6]. However, interpretation of the earlier measurements was complicated by highly nonuniform electron beam pumping. For the scaled device described here, little evidence of

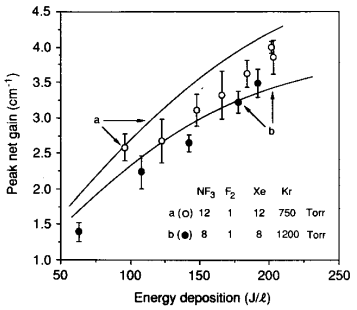

Fig. 17. Measured and computed XeF($C \rightarrow A$) peak gain at 486.8 nm as a function of electron beam energy deposition. The gain probe was translated parallel to the optical axis and the corresponding energy deposition was determined using measurements such as those presented in Fig. 4.

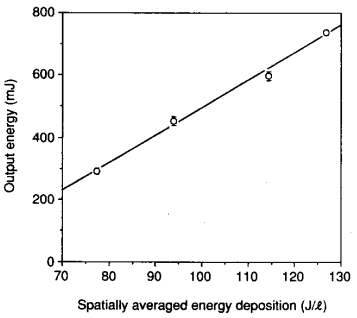

Fig. 18. Injection controlled XeF($C \rightarrow A$) laser output energies measured using an internal $M = 1.7$ unstable resonator and the gas mixture conditions given for Fig. 17 (curve a). The spatially averaged energy deposition in the laser volume, as measured with chlorostyrene film, was varied by adjusting the charging voltage on the electron beam generator Marx capacitors. The four measured points correspond to charging voltages of 65, 75, 85, and 95 kV. A linear relationship was observed with no indication of saturation. This suggests that an increase in the observed specific energy density could be achieved using even higher electron beam pumping rates than available with the current apparatus.

gain saturation was observed as the gain continued to increase up to an energy deposition of 200 J/L corresponding to a pumping rate of 20 MW/cm^3. To verify that the injection controlled laser output reflected the trend in the measured gain, the charging voltage of the Marx bank capacitors of the electron beam machine was varied between 65 and 95 kV in order to adjust the energy deposition throughout the gas volume. As shown in Fig. 18, over a spatially averaged energy deposition range from 75 to 125 J/L a nearly linear dependence of laser energy was observed, with no apparent indication of saturation or the occurrence of a peak in the intrinsic efficiency.

V. Summary and Discussion

Scaling of the high current density electron beam pumped XeF($C \rightarrow A$) excimer laser from an active volume of ~0.02 L to one of ~0.5 L has been successfully demonstrated. Using an internal resonator with a magnification of 1.7, an optimized five-component gas mixture, and an injection intensity of ~3 MW/cm^2 (~2 mJ),

laser output energies in the range of 0.75–0.85 J were measured at 486.8 nm, a wavelength near the maximum of the XeF($C \rightarrow A$) gain spectrum. This corresponds to an energy density of 1.7 J/L and an intrinsic efficiency of 1.3%, compared to maximum values of 1.6 J/L and 1.5% for similar average energy deposition and injection intensity using the 0.02 L laser system [6]. Moreover, the increased single-pass gain of the scaled laser permitted the use of *external* optics with only a small penalty in energy extraction efficiency. We believe that this is the first operation of a XeF($C \rightarrow A$) laser with an *external* resonator.

A. Scaling

A significant aspect in the scaling of the XeF($C \rightarrow A$) laser to larger active volumes was an increased level of competition by oscillation on the KrF($B \rightarrow X$) 248 nm transition. With the increased dimensions of the laser resonator, the spectral properties of the reflective coatings became less effective in the suppression of this competition. However, relatively minor adjustments in gas mixture composition, specifically increases in the partial pressure of Xe and Kr as well as an increase in the ratio of NF_3 to F_2, effectively quenched laser action at 248 nm. This resulted in energy extraction efficiencies at the level that had been demonstrated previously for the small-scale device. Further scaling of the laser length may require additional mixture adjustments to maintain the kinetic suppression of KrF.

Detailed mapping of the spatial distribution of electron beam energy deposition through the pumped gas volume in the direction of electron propagation and an increased uniformity in energy deposition along the direction of the optical axis permitted accurate determination of the dependence of small-signal gain on energy deposition. The results of these experiments have led to a revised understanding of XeF electron quenching. Electron quenching was formerly believed to limit efficient electron beam pumping of the XeF($C \rightarrow A$) laser to deposition levels of ~ 100 J/L using a short (~ 10 ns), high current density excitation pulse. However, the present measurements (Fig. 17) indicate that the onset of saturation in the small-signal gain does not occur until the deposition levels reach ~ 200 J/L (~ 20 MW/cm^3). Thus, it can be concluded that further increases in the specific energy density of the XeF($C \rightarrow A$) laser could be obtained by increasing the electron pumping current densities to values even higher than those available in the current apparatus. This is a significant finding with regard to future scaling of the XeF($C \rightarrow A$) laser beyond the levels we have presently demonstrated.

B. Electron Beam Excitation

The recent reports of efficient XeF($C \rightarrow A$) laser energy extraction using low power density, ~ 250 kW/cm^3 in ~ 700 ns [4] and intermediate power density, ~ 1 MW/cm^3 in 250 ns [3] electron beam pumping demonstrate that efficient XeF($C \rightarrow A$) laser operation is *relatively* insensitive to the electron beam excitation conditions. Indeed, the values of intrinsic laser efficiency and volumetric energy density reported for long pulse excitation are comparable to those reported here, for which the electron beam power density and temporal duration were nearly two orders of magnitude larger and smaller, respectively. Moreover, since the technology is well developed for both *high-* and *low-*power electron beam excitation (short and long pulse durations), scaling considerations should not influence the excitation format to a significant degree. Rather, the choice between short pulse and long pulse XeF($C \rightarrow A$) lasers will in most cases be determined by the application. The high-power pumping format presented here results in net gains which are large over a ~ 50 nm bandwidth ($> 2\%$/cm) and is therefore ideally suited for applications that require efficient, high beam quality, narrow-band operation which is continuously tunable over a wide wavelength range.

ACKNOWLEDGMENT

The authors would like to acknowledge the valuable technical assistance of J. R. Hooten of Rice University.

REFERENCES

[1] W. L. Nighan, R. Sauerbrey, Y. Zhu, F. K. Tittel, and W. L. Wilson, "Kinetically tailored properties of electron-beam excited XeF($C \rightarrow A$) and XeF($B \rightarrow X$) laser media using an Ar–Kr buffer mixture," *IEEE J. Quantum Electron.*, vol. 23, pp. 253–261, 1987.

[2] G. J. Hirst, C. B. Dane, W. L. Wilson, R. Sauerbrey, F. K. Tittel, and W. L. Nighan, "Scaling of an injection-controlled XeF($C \rightarrow A$) laser pumped by a repetitively pulsed, high current density electron beam," *Appl. Phys. Lett.*, vol. 54, pp. 1851–1853, 1989.

[3] P. J. M. Peters, H. M. J. Bastiaens, W. J. Witteman, R. Sauerbrey, C. B. Dane, and F. K. Tittel, "Efficient XeF($C \rightarrow A$) laser excited by a coaxial *e*-beam at intermediate pumping rates," see this issue, pp. 1569–1573.

[4] A. Mandl and L. H. Litzenberger, "Efficient, long pulse XeF($C \rightarrow A$) laser at moderate electron beam pump rate," *Appl. Phys. Lett.*, vol. 53, pp. 1690–1692, 1988; OE/LASE '90, Los Angeles, CA, January 1990.

[5] C. B. Dane, S. Yamaguchi, T. Hofmann, R. Sauerbrey, W. L. Wilson, and F. K. Tittel, "Spectral characteristics of an injection controlled XeF($C \rightarrow A$) excimer laser," *Appl. Phys. Lett.*, vol. 56, pp. 2604–2607, 1990.

[6] N. Hamada, R. Sauerbrey, W. L. Wilson, Jr., F. K. Tittel, and W. L. Nighan, "Performance characteristics of an injection-controlled electron-beam pumped XeF($C \rightarrow A$) laser system," *IEEE J. Quantum Electron.*, vol. 24, pp. 1571–1578, 1988.

[7] S. Lloyd, Y. G. Chen, G. McAllister, M. Montgomery, T. Olson, J. Shannon, B. Dane, G. Hirst, R. Sauerbrey, F. Tittel, and W. Wilson, "A 500 kV rep-rate electron beam generator," in *Proc. Seventh IEEE Pulsed Power Conf.*, Monterey, CA, 1989.

[8] W. P. Bishop, K. C. Humpherys, and P. T. Randike, "Poly(halo)styrene thin-film dosimeters for high doses," *Rev. Sci. Instrum.*, vol. 44, pp. 443–452, 1973.

[9] G. J. Hirst, C. B. Dane, R. Sauerbrey, W. L. Wilson, and F. K. Tittel, "Scaling demonstration of the XeF($C \rightarrow A$) laser," *Metal Vapor, Deep Blue, and Ultraviolet Lasers*, Proc. SPIE, vol. 1041, pp. 149–154, 1989.

[10] C. B. Dane, Th. Hofmann, G. J. Hirst, S. Yamaguchi, R. Sauerbrey, and F. K. Tittel, "Optimization of an injection controlled excimer laser guided by analytical modeling," to be published.

[11] W. L. Nighan and M. C. Fowler, "Kinetic processes in XeF($C \rightarrow A$) laser media excited by a high current density electron beam," *IEEE J. Quantum Electron.*, vol. 25, pp. 791–802, 1989.

[12] N. Hamada, R. Sauerbrey, and F. K. Tittel, "Analytical model for injection-controlled excimer laser amplifiers," *IEEE J. Quantum Electron.*, vol. 24, pp. 2458–2466, 1988.

C. Brent Dane, for a photograph and biography, see this issue, p. 1573.

Graeme J. Hirst was born in London, England, on September 28, 1958. He received the B.A. degree in physics in 1980 and the D.Phil. degree in 1987 from the University of Oxford, England.

After further postdoctoral work in Oxford, he spent a year at Rice University, Houston, TX, working on visible excimer laser development. He returned to England in 1989 to accept an appointment with the S.E.R.C. Rutherford Appleton Laboratory, where he is employed in the Central Laser Facility. His research interests include the physics and chemistry of the rare-gas halides and the development of pulsed-power systems to drive excimer lasers. He is presently occupied with the design of large electron-beam generators.

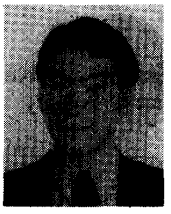

Shigeru Yamaguchi was born in Tokyo, Japan, on December 8, 1958. He received the B.S. and M.S. degrees from Keio University, Yokohama, Japan.

Since 1984 he has been a Research Scientist with Ishikawajima-Harima Heavy Industries Co., Ltd., Tokyo, Japan. In 1989, he joined Rice University, Houston, TX, as a Research Associate. His research interests include high-power gas flow and chemical lasers and their applications.

Mr. Yamaguchi is a member of the Laser Society of Japan.

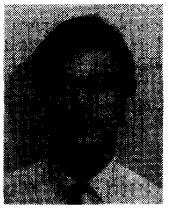

Thomas Hofmann was born in Hannover, Germany, on August 20, 1962. He received the M.S. degree in physics from the University of Hannover in 1988.

In 1988 he joined the Department of Electrical and Computer Engineering, Rice University, Houston, TX, where he is now a graduate student. His research interests include optical thin films and excimer laser development.

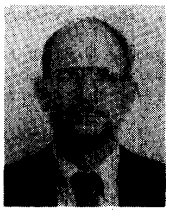

William L. Wilson, Jr. (S'68-M'71-SM'87) was born on February 6, 1943. He received the B.S. degree in 1965, the M.E.E. degree in 1966, and the Ph.D. degree in 1972, all in electrical engineering and all from Cornell University, Ithaca, NY.

From 1971 to 1972, he was an Instructor-Research Associate with the Electrical Engineering School at Cornell. From 1972 to the present, he has been associated with the Department of Electrical and Computer Engineering, Rice University, Houston, TX, where he now holds the position of Professor. His research interests include tunable excimer lasers and solid-state devices.

Dr. Wilson is a member of Tau Beta Pi, Eta Kappa Nu, Sigma Xi, the IEEE Magnetics Society, the IEEE Microwave Theory and Techniques Society, the IEEE Electron Devices Society, and the American Physical Society.

Roland Sauerbrey (M'85), for a photograph and biography, see this issue, p. 1573.

Frank K. Tittel (SM'72-F'86), for a photograph and biography, see this issue, p. 1573.

William L. Nighan (SM'85) was born in Philadelphia, PA, in 1938. He received the B.S. degree in engineering from the University of Dayton, Dayton, OH, in 1961 and the M.S. degree in engineering science from Northwestern University, Evanston, IL, in 1962.

Since 1962 he has been with the United Technologies Research Center, East Hartford, CT, where he is Manager of Applied Physics in the Electronics and Photonics Technologies Department. His primary research activities have been in areas of gas discharge physics, electric lasers, plasma displays, and applied atomic, molecular, and chemical physics.

Mr. Nighan is a member of Sigma Xi, Tau Beta Pi, and the American Physical Society.

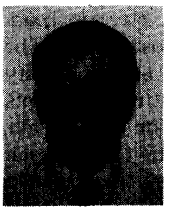

Michael C. Fowler was born in New York, NY, in 1941. He received the B.S. degree in chemistry from Yale University, New Haven, CT, in 1963 and the Ph.D. degree in physical chemistry from the Massachusetts Institute of Technology, Cambridge, MA, in 1967.

Since 1969, he has been with the United Technologies Research Center, East Hartford, CT, where he is now a Senior Research Scientist in the Combustion and Environmental Science group. His research activities have included both experimental and analytical work in the fields of plasma physics, electric discharge laser physics, optics and problems associated with high-power laser propagation, and chemical methods of hydrogen storage.

Dr. Fowler is a member of Sigma Xi, Alpha Chi Sigma, the American Physical Society, the Optical Society of America, and the Society of Photo-Optical Instrumentation Engineers.